JAAS

PAPER

View Article Online
View Journal | View Issue

Lead isotope analysis of melt inclusions by LA-MC-ICP-MS†

Cite this: *J. Anal. At. Spectrom.*, 2014, **29**, 1393

Le Zhang,[ab] Zhong-Yuan Ren,*[a] Alexander R. L. Nichols,[c] Yin-Hui Zhang,[ab] Yan Zhang,[ab] Sheng-Ping Qian[ab] and Jian-Qiang Liu[ab]

Pb isotope compositions of melt inclusions provide unique information about the composition of primary magmas and their source. In this study, we have developed a method for measuring Pb isotopes in small olivine-hosted melt inclusions (>40 μm) from young and old volcanoes by LA-MC-ICP-MS. We used a new interface cone assemblage consisting of a Jet sample cone and X skimmer cone. A small flow of N_2 gas was added to the carrier gas and passed through the assemblage to enhance the signal intensity. In addition the energy and repetition rate of the laser conditions were reduced and the signal integration time was shortened in order to lengthen the laser ablation time and to collect enough data. Mass bias and instrument drift were corrected using a standard–sample–standard bracketing method. The analysis routine employed eight ion counters to receive ^{238}U, ^{235}U, ^{232}Th, ^{208}Pb, ^{207}Pb, ^{206}Pb, ^{204}Pb and ^{202}Hg signals simultaneously, which allowed Hg interference to be corrected on ^{204}Pb, and in old samples U–Th decay to be age-corrected. Using the Jet and X cones, under the same laser ablation conditions, the precisions for almost all the measured standard glasses are improved by at least a factor of two compared to using standard cones. At ^{208}Pb signal intensity >200 000 cps, external precisions of ratios involving ^{204}Pb are better than 1.3% (2RSD) and precisions of $^{208}Pb/^{206}Pb$ and $^{207}Pb/^{206}Pb$ are better than 0.23% (2RSD). The results of Pb isotopes in olivine-hosted melt inclusions, using 45 μm laser spots, show that the internal precisions of $^{208}Pb/^{206}Pb$ and $^{207}Pb/^{206}Pb$ for most analyzed melt inclusions are better than 0.2% (2RSE) and for ratios involving ^{204}Pb are better than 0.8% (2RSE). We are able to present the first ever Pb isotope data from ~260 Ma Emeishan flood basalt olivine-hosted melt inclusions. They show the importance to do age correction which results in the reduction of the spread of data in old samples. The mean values of age-corrected $^{208}Pb/^{206}Pb$ and $^{207}Pb/^{206}Pb$ have 1.2% and 2.8% deviations from the uncorrected mean values, respectively. The method developed here provides a fast, precise and accurate *in situ* Pb isotopic composition analysis, applicable not only to melt inclusions from young basalts, but also from old samples that require correction for U–Th decay.

Received 3rd March 2014
Accepted 1st April 2014

DOI: 10.1039/c4ja00088a

www.rsc.org/jaas

Introduction

Melt inclusions are small parcels of melt trapped in crystals during magma evolution.[1–5] Compared to the whole rock, melt inclusions provide several advantages: (1) if last equilibrated at higher pressures than those of eruption, melt inclusions can retain volatiles (H, C, Cl, S, F) and may provide the easiest way to measure these elements; (2) melt inclusions may represent primitive melts trapped in the early stages of magma evolution, and they may also preserve a wider diversity of melt compositions than are represented by the bulk host rocks; (3) in altered rocks, melt inclusions within resistant phenocryst phases may be protected from alteration, providing a useful method for producing less potentially ambiguous results to determine the composition of magmas in these whole rocks.[4] The Pb isotope composition of melt inclusions can provide important information on the origin of mafic lavas.[3–6] So far, the Pb composition measurement of melt inclusions has been mainly performed using Secondary Ion Mass Spectrometry (SIMS).[3,6–9] However, this approach is hampered by very high instrument cost (thus SIMS is not as widespread as LA-ICP-MS), limited analytical machine time for users, and high analysis cost. In recent years, laser ablation multiple-collector inductively coupled plasma mass spectrometry (LA-MC-ICP-MS) has become a powerful alternative method, as it can conduct *in situ* isotope analyses rapidly and at lower cost than SIMS. Because of these advantages, this technology has quickly been adopted for

[a]*State Key Laboratory of Isotope Geochemistry, Guangzhou Institute of Geochemistry, Chinese Academy of Sciences, Guangzhou 510640, China. E-mail: zyren@gig.ac.cn; Fax: +86-20-85291510; Tel: +86-20-85292969*

[b]*University of Chinese Academy of Sciences, Beijing 100049, China*

[c]*Institute for Research on Earth Evolution (IFREE), Japan Agency for Marine Earth Science and Technology (JAMSTEC), 2-5 Natsushima-cho, Yokosuka, Kanagawa 237-0061, Japan*

† Electronic supplementary information (ESI) available. See DOI: 10.1039/c4ja00088a

in situ Pb-isotope analysis. For example, Paul *et al.*[10] using a 93 μm laser spot analyzed the Pb isotopic composition of glass standards. Kent[11] made a comparison between the Faraday cup and ion counting systems for Pb-isotope analysis and argued that the precision is strongly dependent on ion intensities. Souders and Sylvester[12] using a 40–99 μm laser spot analyzed several glass standards with different Pb contents. Though analysis data from these studies have a good precision and accuracy, such large spot sizes or high repetition rates and strong laser energy (*e.g.* 93 μm, 6 Hz, 5 J cm^{-2} reported by Paul *et al.*;[10,13] and 40–99 μm, 10 Hz, 5 J cm^{-2} reported by Souders and Sylvester[12]) are difficult to apply to most melt inclusions because the inclusions will be fully penetrated in only a few seconds. Most melt inclusions are small and cannot be analyzed using a large laser spot (*i.e.*, >80 μm). In order to analyze Pb isotopes by LA-MC-ICP-MS in melt inclusions, the laser spot size, repetition rate and energy must be carefully adjusted to maximize the laser ablation time in order to obtain data of high precision. In this study, we have developed an analytical protocol for *in situ* measurements of Pb isotopes in relatively small (diameter > 40 μm) geological samples by LA-MC-ICP-MS. Using this protocol we undertook *in situ* analysis of Pb isotopes in several glass standards with different Pb contents (1.7–16 μg g^{-1}). In addition, we present Pb isotopic compositions of olivine-hosted melt inclusions from Cenozoic Hainan Island basalts erupted between ~17 Ma and ~0.1 Ma ago and end-Permian Emeishan flood basalts erupted ~260 Ma ago.

Instruments

All analyses were performed using a Thermo Fisher Scientific Neptune Plus MC-ICPMS at the Guangzhou Institute of Geochemistry, Chinese Academy of Sciences. This machine is a double focusing multi-collector ICP-MS and has the capability of high mass resolution measurements in multiple collector mode. It is equipped with eight variable position Faraday cups and one fixed central Faraday cup, and eight ion counters (three of them are secondary electron multipliers and the others are compact discrete dynamic multipliers). This collector system can analyze isotopic ratios with a relative mass range of 17%, allowing simultaneous acquisition of ion signals ranging from mass ^{202}Hg to ^{238}U. This machine is also equipped with a newly designed large dry interface pump (100 m^3 h^{-1} pumping speed), which results in an increase in sensitivity. In addition, the newly designed interface cone assemblage consisting of a Jet sample cone and X skimmer cone (from Thermo Scientific) also significantly improves the instrument sensitivity. This machine can work in static mode or peak jump mode, in our experiment, however only the static mode was used.

The laser ablation system, Resonetics RESOlution M-50, includes: (1) a 193 nm Lambda Physik ComPex Pro 110 ArF excimer laser with a pulse width of *ca.* 20 ns; (2) a sample ablation stage that can hold four mounts at the same time; and (3) a high precision computer controlled sample positioning system. The laser spot size can vary from 5 to 380 μm, the repetition rate from 1 to 20 Hz and the energy from 80 mJ to 180 mJ. In order to weaken the laser energy, 25% and 50% energy attenuators are installed on the laser path which can change the laser energy density from ~2 J cm^{-2} to 18 J cm^{-2}. This allows samples with different sizes and different abundances of elements of interest to be measured. A "squid" smoothing device on the gas line to the ICP gives a smooth signal. The system can wash out 99% of the signal in less than 1.5 seconds due to its innovative sample cell design. Helium is used as the carrier gas to enhance transport efficiency and minimize deposition of ablated material.[14–16] A small amount of N_2 is added to the sample gas using a Y-shape connector to enhance the sample signal.

Samples

Glass standards

The standard glasses used in this study include: two NIST reference glasses, NIST 612 (38.6 μg g^{-1} Pb)[17] and NIST 614 (2.32 μg g^{-1} Pb);[17] two GSJ reference glasses, JB-1 (3.5 μg g^{-1} Pb)[17] and JB-2 (<1 μg g^{-1} Pb);[18] and three USGS reference glasses, BHVO-2G (1.7 μg g^{-1} Pb),[17] NKT-1G (3.01 μg g^{-1} Pb)[19] and TB-1G (16 μg g^{-1} Pb).[20] JB-1, JB-2, BHVO-2G and TB-1G are made from basalt powders and NKT-1G is made from peralkaline basalt powder, whereas NIST 612 and NIST 614 are synthetic standards.[21,22] Table 1 shows the major element composition of these standard glasses. Small chips of each selected standard glass were mounted in one-inch diameter epoxy resin mounts. The mounts were polished to an even sample surface using diamond abrasive. To eliminate any potential surface contamination of the samples, each mount was cleaned in an ultrasonic bath with ~2% depurated nitric acid three times and rinsed with double-distilled Milli-Q water, and then the mount was dried with a nitrogen jet.

Melt inclusions

We handpicked olivine grains from crushed and sieved samples. To determine the Pb composition of melt inclusions, it is preferable to analyze a homogeneous glass rather than a mixture of various crystalline phases and residual glass.[3,4,23] In order to reduce the "matrix effect" between melt inclusions and glassy standards, prior to *in situ* Pb isotope analysis, the melt inclusions containing mixtures of crystals and glass require reheating and quenching in order to rehomogenize them as entirely glassy inclusions.[1–3] We reheated olivine grains and homogenized melt inclusions using 1 atm furnaces at 1250 degree centigrade for 10 min in QFM-buffer condition, and then quenched and polished them until the melt inclusions were exposed at the surface. All sample preparation was performed at the melt inclusion laboratory in the State Key Laboratory of Isotope Geochemistry, Guangzhou Institute of Geochemistry, Chinese Academy of Sciences (GIG-CAS). The preparation procedure of melt inclusions is described in detail by Ren *et al.*[23]

Statistics of nearly 1500 olivine-hosted melt inclusions from basalt-picrites from Hawaii (508), Hannuoba (North China craton, 343), Emeishan (296) and Hainan (301) show that about 42% of these melt inclusions have a diameter larger than 40 μm (short dimensions). Only 9.5% of these melt inclusions have a

Table 1 The chemical compositions of the standard glasses used in this study[a,b]

	Provider	SiO_2	TiO_2	Al_2O_3	FeOt	MgO	CaO	Na_2O	K_2O	Pb	$^{208}Pb/^{206}Pb$	$^{207}Pb/^{206}Pb$	$^{208}Pb/^{204}Pb$	$^{207}Pb/^{204}Pb$	$^{206}Pb/^{204}Pb$
JB-1	GSJ	53.15	1.32	14.53	8.09	7.71	9.25	2.77	1.43	3.5	2.1058	0.8480	38.644	15.561	18.351
JB-2	GSJ	53.25	1.19	14.64	10.28	4.62	9.82	2.04	0.42	<1	2.0868	0.8484	38.278	15.562	18.343
NIST 612	NIST	72.1	0.01	2.03	0.01	0.01	11.9	13.7	0.02	38.57	2.1645	0.9073	37.000	15.510	17.094
NIST 614	NIST	72.1	0.001	2.04	0.002	0.01	11.9	13.7	0.01	2.32	2.1013	0.8710	37.4723	15.533	17.83
TB-1G	USGS	53.7	0.85	17.05	8.387	3.6	7.04	3.36	4.5	16	2.1063	0.8482	38.6153	15.551	18.33
NKT-1G	USGS	38.68	3.95	10.2	12.00	14.33	13.21	3.48	1.28	3.1	1.9992	0.7955	39.215	15.604	19.615
BHVO-2G	USGS	49.8	2.79	13.6	11.3	7.23	11.4	2.4	0.51	1.7	2.0524	0.8345	38.211	15.536	18.617

[a] The major and trace element compositions of NIST 612, NIST 614, JB-1 and BHVO-2G are from ref. 17. For TB-1G and NKT-1G are from ref. 19 and 20. For JB-2 are from ref. 18. Preferred reference lead ratio values for NIST 614 are from ref. 36, for NKT-1G and TB-1G are from ref. 34, for JB-2 and BHVO-2G are from ref. 35 and for JB-1 are from ref. 36. [b] The oxides are in wt% and the lead is in ppm.

diameter larger than 80 μm (Fig. 1). Whereas the Hainan Island basalts were erupted in the Cenozoic and have a relatively young age, the Emeishan flood basalts are older having been erupted at the end of the Permian (~260 Ma) and the effect of U–Th decay on the Pb isotopic composition of their melt inclusions needs to be considered.

Analytical method

Hg may exist in Ar, He and N_2 gases, and ^{204}Hg has significant isobaric interference on ^{204}Pb.[10,12,24] To reduce ^{204}Hg interference, three Au-coated glass wool Hg filters (VICI Metronics) were placed on the gas lines to the ablation cell to filter Hg from Ar, He and N_2 gases. All gas tubes were rinsed with ~10% purified nitric acid (HNO_3) and rinsed again with double-distilled Milli-Q water. After this, the gas tubes were dried by ultra pure N_2 gas flow. Other instrument components such as the cones and torch were washed with an ultrasonic cleaner in ~0.1% distilled nitric acid for 20 minutes and then diluted by distilled Milli-Q water, before drying under ultra pure N_2 gas flow.

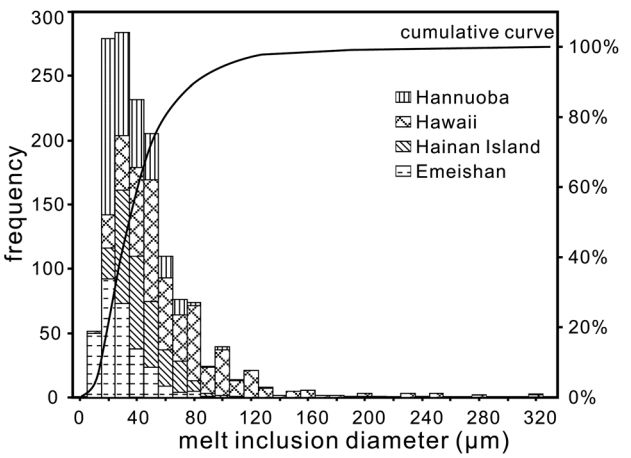

Fig. 1 Statistics of olivine-hosted melt inclusion sizes. These olivine-hosted melt inclusions are from basalts in the Hannuoba (343), Hainan (301), Emeishan LIP (296) and Hawaii (508) volcanoes. 42% of the melt inclusions have diameters larger than 40 μm; only 9.5% melt inclusions are larger than 80 μm.

The gain factors for new Channeltrons need a "burn-in" period (several months to years) for stabilization.[20,24] The instrument used in our study had run for more than one year when we performed these analyses. Over this time the gain factors for ion counters (ICs) used in this study have become stable. Prior to each analytical period, the relative yield values for each IC were determined, referenced to IC1 under peak jump mode. After an ~40 minute warm-up period, gas flow, torch position, lens focus potentials, peak overlap and peak center were checked and adjusted. Then the yield values were measured in solution mode with an integration time of 4.194 s. A low ^{238}U signal (~3 mV/187 500 cps) from the Neptune tune solution was used. The ^{238}U signal entered in the eight ICs sequentially under different magnetic fields. The measurement of yield values included 10 blocks, and each block had 10 cycles. The yield values for each IC were then determined by normalizing the measured signal intensities for each IC to IC1. If the relative yield values are not within 80% of IC1, the operation voltage on the IC is improved. During almost 2 hours relative yield determination for each IC, the uncertainty of the yield value for each IC was less than 1.5% (2RSD).

The gas flow, torch position, lens focus potentials, peak overlap and peak center were checked and adjusted to achieve a typical ^{208}Pb sensitivity of 95 000 cps per μg g^{-1} Pb with standard cones assemblage for *in situ* analyses of NIST 614 with a 32 μm and 10 Hz repetition rate laser spot. The ^{208}Pb signals of all samples were limited larger than 100 000 cps to ensure a reasonable analytical precision and not more than 500 000 cps to prolong the lifetime of the ICs and to limit the IC drift through adjusting laser parameters. Under the normal 45 μm laser spot used in our study, the 100 000–500 000 cps ^{208}Pb intensity corresponds to about 1–6 μg g^{-1} Pb content which ensures a reasonable analytical precision. However, if the sample has a Pb content more than 6 μg g^{-1}, we can change the laser spot to smaller size (from 45 μm to 33 μm) to reduce the signal intensity. During our experiment, gas blanks for ^{202}Hg and ^{208}Pb were ~4000 cps and <100 cps when using the standard cones assemblage. When using the Jet sample cone and X skimmer cone, the instrument sensitivity was improved and the intensities of gas blanks for ^{202}Hg and ^{208}Pb rose to ~4000–9000 cps and <200 cps. Typical instrument operating parameters and the collector configuration for the analysis of Pb isotopes are listed in Tables 2 and 3.

Table 2 Laser ablation and LA-MC-ICPMS instrumentation parameters

MC-ICP-MS	
Instrument	Neptune Plus
RF power	1250 W (optimized daily)
Auxiliary gas (Ar)	0.98 L min^{-1} (optimized daily)
Sample gas (Ar)	0.92 L min^{-1} (optimized daily)
Cooling gas (Ar)	16.00 L min^{-1}
Measurement mode	Static
Interface cones	Ni standard cones
	Jet sample cone + X skimmer cone
Acceleration voltage	10 kV
Detection system	Eight ion counters
Integration time	1.049 s/0.131 s/0.262 s
Laser ablation system	
Instrument	RESOlution M-50
Beam	UV 193 (ArF excimer)
Spot size	13–45 μm
Repetition rate	3–10 Hz
Energy density	8–9 J cm^{-2}/4 J cm^{-2}/2.3 J cm^{-2}
Attenuation	Not used/25%/50%
Ablation time	50 s/30 s
Blank time	40 s/30 s
He gas to cell	800 mL min^{-1}
N_2 gas to cell	2 mL min^{-1}

All time-resolved raw data were exported from the MC-ICP-MS in ASCII format with Neptune Plus software and processed off-line using a spreadsheet program created by the authors. First, the mean gas background intensities were subtracted from the raw time-resolved signal intensities for each isotope. Then the isobaric interference of ^{204}Hg, which was calculated with the measured ^{202}Hg intensity and the natural ^{204}Hg/^{202}Hg ratio (0.2301 (ref. 25)), was subtracted from ^{204}(Pb + Hg) to obtain the net ^{204}Pb signal intensity. Finally all isotope ratios were calculated and corrected for mass bias and instrumental drift with a standard–sample–standard bracketing method and any outliers (>±2SD; standard deviation) were excluded. The following gives a detailed description of the data reduction techniques.

Mass bias correction

Among the four Pb isotopes (^{208}Pb, ^{207}Pb, ^{206}Pb and ^{204}Pb), ^{208}Pb, ^{207}Pb and ^{206}Pb are derived from the radioactive decay of U and Th and only ^{204}Pb is an invariant isotope. As a result for Pb isotope analysis, there is no invariant isotope pair to make a mass bias correction as is performed in Sr, Nd and Hf isotope systems. One strategy is to aspirate a Tl tracer solution during laser analysis to monitor Pb fractionation.[26,27] Another strategy is to use standard materials to make external corrections.[10–12] Because the configuration of the ion counters in the instrument used in this study does not allow the signals of Tl, Pb and Hg to be received simultaneously the mass bias correction was performed using the latter method. The Pb isotope measurement of every unknown sample was preceded and followed by once measurement of standard glass, and using the follow equation:

$$S_c = \frac{S_m}{(R_{m1} + R_{m2})/2/R} \quad (1)$$

where S_m is the measured value on the unknown sample; R_{m1} and R_{m2} are the measured values on the analysis of the standard glass preceding and following the unknown, respectively; and R is the preferred reference value, and the final corrected value (S_c) was calculated.

Results and discussion

Measurement of standard solutions

NBS 981 standard solution and the Neptune standard solution were used to evaluate the accuracy and precision of the instrument during Pb isotope analysis. NBS 981 was used as an external standard whereas the Neptune solution was the "unknown sample". The two solutions were analyzed in turn and the Neptune solution's Pb isotope ratios were corrected using eqn (1). We measured two Neptune solutions with different Pb contents (one where the ^{208}Pb signal intensity was 190 000 cps (counts per second) and the other where it was 32 000 cps), and using two different integration times (0.131 and 1.049 s). An integration time of 0.131 s allowed 600 cycles of data to be obtained; 1.049 s allowed 90 cycles of data to be obtained (ESI S1†).

The results show that ^{208}Pb/^{206}Pb and ^{207}Pb/^{206}Pb of the Neptune solution with 190 000 cps ^{208}Pb intensity have external precisions (2 relative standard deviation, 2RSD; $n = 40$) better than 0.15% and both are within 0.02% of the preferred values. ^{20x}Pb/^{204}Pb ($x = 6$, 7 or 8) of the same solution have external precisions better than 0.31% (2RSD) and are within 0.05% of the preferred values. The Pb isotope ratios of the Neptune solution with a ^{208}Pb intensity of 32 000 cps are just slightly less precise than that of the other solution (for example, with an integration time of 1 s the precision of ^{207}Pb/^{206}Pb of the solution with 190 000 cps ^{208}Pb intensity is 0.0006 (2SD) and under the same instrument conditions, the precision of the solution with 32 000 cps ^{208}Pb intensity is 0.0014 (2SD)). At the same signal intensity, the precision of data with an integration time

Table 3 Neptune Plus collector configuration for Pb isotope analysis

Collector[a]	IC5	IC4	IC3	IC2	IC1	C	IC6	IC7	IC8
	^{202}Hg	^{204}(Pb + Hg)	^{206}Pb	^{207}Pb	^{208}Pb	224.10	^{232}Th	^{235}U	^{238}U

[a] IC1 to IC8 are ion counters and C is the center Faraday cup.

of 1 s is slightly better than that with an integration time of 0.131 s. The internal precision of data for the solution with 32 000 cps ^{208}Pb intensity is twice as large as those for the solution with a 190 000 cps ^{208}Pb intensity. This indicates that prolonging integration time and raising signal intensity can improve the analysis precision. The instrument has good stability and data reproducibility and the external correction used to correct instrument drift and mass bias is robust.

Correlation between internal precision and ablation time

To better understand the relationship between the internal precision and the ablation time we analyzed the Pb isotopic composition of NKT-1G over different ablation times (5, 10, 15, …, 60 s). Three analyses were performed using each ablation time and then averaged (Fig. 2). As the ablation time increases the precision improves. When the ablation time is less than 20 s, the precision deteriorates quickly (the standard errors (SE) of ^{208}Pb/^{204}Pb and ^{208}Pb/^{206}Pb are larger than 0.17 and 0.0012 respectively), whereas above 30 s there is little improvement. Based on this fact, an ablation time of 30 s was chosen to ensure data with good internal precision and that most melt inclusions larger than 40 μm in diameter would not be fully penetrated.

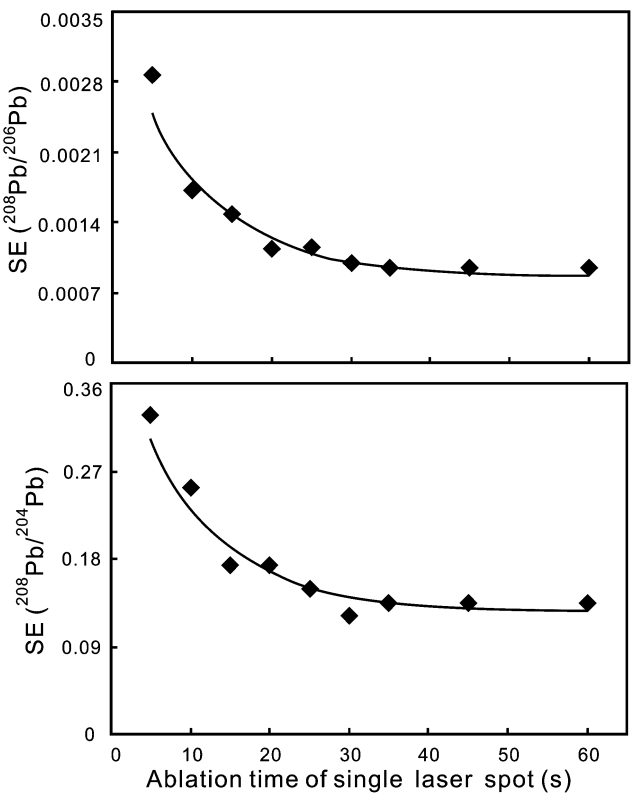

Fig. 2 Relationship between the internal precision of single spot analysis and the ablation time for NKT-1G. As the laser ablation time increases, the internal precision improves. When the ablation time of a single laser spot is longer than 30 s, the precisions of Pb isotope ratios stabilize. The laser parameters are 45 μm spot, 3 Hz repetition rate and 80 mJ energy with a 25% energy attenuator (~2.3 J cm^{-2} energy density). A Jet sample cone and X skimmer cone were used. Under these laser ablation conditions the ^{208}Pb intensity of NKT-1G is about 260 000 cps.

Using the standard sample cone and skimmer cone, the signal intensities of samples with low Pb content (<10 μg g^{-1}) are relatively low and the precisions of ratios involving ^{204}Pb are poor. The assemblage of a Jet sample cone and X skimmer cone can significantly improve the sample signal.[28,29] As a result both the standard cones assemblage and the Jet and X cones assemblage were used to measure the same samples and compared to assess data precision and accuracy.

Standard cones assemblage

In order to compare our results with previous LA-MC-ICPMS results at a similar signal intensity, Pb isotopes of NIST 614 and NKT-1G were analyzed using a standard cones assemblage and laser parameters optimized to obtain the same signal intensities as in previous studies.

The laser parameters were adjusted (spot size: 32 μm; repetition rate: 10 Hz; energy: 100 mJ; energy density: 9 J cm^{-2}; integration time: 1.049 s) to achieve 220 000 cps ^{208}Pb signal intensity (5800 cps for ^{204}Pb) for NIST 614 (2.32 μg g^{-1} Pb), similar to that of MPI-T1-G in Souders and Sylvester[12] (~240 000 cps) (Table 4 and Fig. 3). The data in six days over two months show that the external precisions (2RSD) of ^{208}Pb/^{206}Pb, ^{207}Pb/^{206}Pb, ^{207}Pb/^{204}Pb, ^{208}Pb/^{204}Pb and ^{206}Pb/^{204}Pb are 0.29%, 0.41%, 0.98%, 0.97% and 0.93%, respectively; a little worse than those reported for MP1-T1-G by Souders and Sylvester[12] (Table 5). This may be caused by the lower signal intensity in this study. The accuracy for ^{208}Pb/^{206}Pb and ^{207}Pb/^{206}Pb is better than 0.07% and for ^{20x}Pb/^{204}Pb, better than 0.45%. Using a laser spot of 32 μm, 10 Hz repetition rate and 80 mJ energy with a 50% energy attenuator (4 J cm^{-2} energy density), NKT-1G (3.01 μg g^{-1} Pb) has a signal intensity of 90 000 cps for ^{208}Pb (2400 cps for ^{204}Pb), which is almost the same as that for MPI-ML3B-G reported by Souders and Sylvester[12] (~86 000 cps). The precisions and accuracies for ^{208}Pb/^{206}Pb and ^{207}Pb/^{206}Pb are ~0.44% (2RSD) and ~0.10% respectively, whereas for ^{20x}Pb/^{204}Pb, they are ~1.70% (2RSD) and ~0.60% (Table 4) which show an improved accuracy and precision compared to the result of MPI-ML3B-G reported by Souders and Sylvester[12] (Table 5).

In order to measure melt inclusions with diameters less than 30 μm, we propose a 23 μm laser spot size, 3 Hz repetition rate and 80 mJ energy with a 50% energy attenuator (energy density is 4 J cm^{-2}). Under these laser conditions, NIST 614 and TB-1G were measured ($n = 110$). The ^{208}Pb signal for NIST 614 is about 22 000 cps (600 cps for ^{204}Pb), the precisions (2RSD) for ^{208}Pb/^{206}Pb, ^{207}Pb/^{206}Pb, ^{207}Pb/^{204}Pb, ^{208}Pb/^{204}Pb and ^{206}Pb/^{204}Pb are 0.64%, 0.79%, 4.05%, 4.25% and 4.17% respectively, and their accuracies are 0.25%, 0.03%, 0.51%, 0.36% and 0.36%, respectively (Table 4 and Fig. 4). Obviously, because the sample signal is much lower, the precisions of ratios involving ^{204}Pb are much worse and the accuracies a little worse compared to the normal setup. For TB-1G, however, the ^{208}Pb signal intensity is relatively high (90 000 cps signal intensity for 16 μg g^{-1} total Pb) resulting in the improvement of

Table 4 Accuracy and precision of lead isotope ratios for samples measured in this study with different laser ablation parameters[a]

Standard cones assemblage	Total Pb	Spot size	Repetition rate	Energy	Energy attenuator	Integration time	Ablation time		$^{208}Pb/^{206}Pb$	$^{207}Pb/^{206}Pb$	$^{208}Pb/^{204}Pb$	$^{207}Pb/^{204}Pb$	$^{206}Pb/^{204}Pb$
NIST 614	2.32 μg g^{-1}	32 μm	10 Hz	100 mJ	Not used	1.049 s	50 s	2RSD n = 111	0.29%	0.41%	0.98%	0.97%	0.93%
								Accuracy	0.06%	−0.01%	−0.35%	−0.41%	−0.41%
NKT-1G	3.01 μg g^{-1}	32 μm	10 Hz	80 mJ	50%	1.049 s	50 s	2RSD n = 20	0.42%	0.44%	1.58%	1.62%	1.72%
								Accuracy	0.03%	−0.13%	−0.48%	−0.62%	−0.54%
TB-1G	16 μg g^{-1}	23 μm	3 Hz	80 mJ	50%	0.262 s	30 s	2RSD n = 18	0.39%	0.36%	1.64%	1.51%	1.64%
								Accuracy	0.20%	0.06%	−0.26%	−0.41%	−0.41%
NIST 614	2.32 μg g^{-1}	23 μm	3 Hz	80 mJ	50%	0.131 s	30 s	2RSD n = 110	0.64%	0.79%	4.05%	4.25%	4.17%
								Accuracy	0.25%	0.03%	0.51%	0.36%	0.36%
Jet + X cones assemblage	Total Pb	Spot size	Repetition rate	Energy	Energy attenuator	Integration time	Ablation time		$^{208}Pb/^{206}Pb$	$^{207}Pb/^{206}Pb$	$^{208}Pb/^{204}Pb$	$^{207}Pb/^{204}Pb$	$^{206}Pb/^{204}Pb$
BHVO-2G	1.7 μg g^{-1}	23 μm	3 Hz	80 mJ	50%	0.262 s	30 s	2RSD n = 20	0.60%	0.50%	5.50%	5.30%	5.20%
								Accuracy	0.03%	−0.05%	1.00%	0.87%	1.02%
NKT-1G	3.01 μg g^{-1}	23 μm	3 Hz	80 mJ	50%	0.262 s	30 s	2RSD n = 16	0.39%	0.35%	3.04%	3.13%	3.13%
								Accuracy	−0.17%	0.02%	−0.77%	−0.60%	−0.70%
TB-1G	16 μg g^{-1}	24 μm	3 Hz	80 mJ	25%	0262 s	30 s	2RSD n = 18	0.19%	0.16%	1.04%	0.88%	0.81%
								Accuracy	−0.13%	−0.12%	−0.41%	−0.27%	−0.22%

[a] Preferred reference values for NIST 614 are from ref. 21, for NKT-1G and TB-1G are from ref. 34, for BHVO-2G are from ref. 35 and for JB-1 are from ref. 36.

Fig. 3 Pb isotope analysis of NIST 614 with 32 μm laser spot size, 10 Hz repetition rate and 9 J cm^{-2} energy density. The preferred values are from ref. 21. The error bars correspond to 1 standard error (1SE).

precisions and accuracies for Pb isotope ratios. The precisions and accuracies for $^{208}Pb/^{206}Pb$ and $^{207}Pb/^{206}Pb$ are ~0.4% (2RSD) and ~0.20%. For $^{20x}Pb/^{204}Pb$, the precisions and accuracies are ~1.60% and ~0.40%, respectively.

Jet sample cone and X skimmer cone assemblage

Compared to the standard sample cone, using the Jet sample cone and X skimmer cone together with a large dry interface pump can improve the signal intensity significantly. With a laser spot size of ~23 μm, repetition rate of 3 Hz, energy density of 4 J cm^{-2}/2.3 J cm^{-2} and a 50%/25% energy attenuator, BHVO-2G, NKT-1G and TB-1G were analyzed with the Jet sample cone and X skimmer cone. The results show that with increasing sample Pb content the data precision improves (Table 4). BHVO-2G, which has the lowest Pb content among the three glasses, had the lowest signal intensity under these laser conditions (~55 000 cps and 1500 cps for ^{208}Pb and ^{204}Pb). This results in poor precision for ratios involving ^{204}Pb, larger than 5.0% (2RSD). NKT-1G, with 3.01 μg g^{-1} total Pb, shows better precisions compared to BHVO-2G. The precisions for ratios involving ^{204}Pb are a little larger than 3.0% and for $^{208}Pb/^{206}Pb$ and $^{207}Pb/^{206}Pb$ they are better than 0.40% (2RSD). TB-1G, which has the highest signal intensity (~420 000 cps and 11 000 cps for

Table 5 Summary of the previous studies

Authors		Total Pb	System	Detector		Repetition rate	Spot size	Ablation time		$^{208}Pb/^{206}Pb$	$^{207}Pb/^{206}Pb$	$^{208}Pb/^{204}Pb$	$^{207}Pb/^{204}Pb$	$^{206}Pb/^{204}Pb$
Saal *et al.*[7]	Loihi glass	3 μg g^{-1}	SIMS				20–30 μm		2RSD	0.66%	0.50%			
Paul *et al.*[10]	BCR-2G	10 μg g^{-1}	MC-ICPMS	Faraday-IC	5 J cm^{-2}	6 Hz	93 μm	60 s	2RSD	0.11%	0.22%	0.38%	0.42%	0.40%
									Accuracy	0.15%	0.12%	0.07%	0.21%	0.21%
	MPI-ATHO	6 μg g^{-1}			5 J cm^{-2}	6 Hz	93 μm	60 s	2RSD	0.30%	0.47%	0.48%	0.59%	0.60%
									Accuracy	0.00%	0.24%	0.04%	0.30%	0.30%
	MPI-KL-2G	2 μg g^{-1}			5 J cm^{-2}	6 Hz	93 μm	60 s	2RSD	0.70%	1.06%	1.47%	1.76%	1.43%
									Accuracy	−0.05%	0.61%	−0.24%	0.88%	0.72%
Kent[11]	BCR-2G	10 μg g^{-1}	MC-ICPMS	Faraday-IC	12 J cm^{-2}				2RSD	0.14%	0.37%	0.41%	0.30%	0.61%
									Accuracy	0.10%	0.12%	−0.05%	0.12%	−0.05%
	NIST 614	2.31 μg g^{-1}							2RSD	0.23%	0.37%	0.54%	0.52%	0.56%
									Accuracy	−0.14%	0.46%	−0.29%	0.44%	−0.12%
Souders and Sylvester[12]	MPI-T1-G	11.6 μg g^{-1}	MC-ICPMS	IC	5 J cm^{-2}	10 Hz	40 μm	50 s	2RSD	0.36%	0.22%	0.83%	0.78%	0.70%
									Accuracy	0.02%	−0.07%	0.03%	−0.04%	0.04%
	MPI-ATHO-G	5.67 μg g^{-1}			5 J cm^{-2}	10 Hz	40 μm	50 s	2RSD	0.31%	0.31%	1.91%	1.98%	2.10%
									Accuracy	0.26%	−0.09%	−0.14%	−0.23%	−0.09%
	MPI-KL2-G	2.07 μg g^{-1}			5 J cm^{-2}	10 Hz	69 μm	50 s	2RSD	0.40%	0.34%	2.59%	2.51%	2.82%
									Accuracy	0.16%	−0.01%	0.15%	0.01%	0.12%
	MPI-ML3B-G	1.38 μg g^{-1}			5 J cm^{-2}	10 Hz	69 μm	50 s	2RSD	0.53%	0.34%	2.71%	2.73%	2.73%
									Accuracy	−0.30%	−0.45%	−1.59%	−1.49%	−1.07%

^{208}Pb and ^{204}Pb), has precisions ~1.0% or better for ratios involving ^{204}Pb, and 0.19% and 0.16% (2RSD) for $^{208}Pb/^{206}Pb$ and $^{207}Pb/^{206}Pb$, respectively; most of these ratios are within 0.30% of the preferred values. Compared to standard cones, using the Jet sample cone and X skimmer cone for TB-1G results in significant improvements in precision (Table 4).

Under the same laser conditions, we compared single spot analyses for NIST 614 using the standard cones assemblage with one using the Jet and X cones. Using the standard cones, the ^{208}Pb signal intensity for NIST 614 is about 22 000 cps, whereas using the Jet and X cones it increases to 65 000 cps (Fig. 5). It is clear that the variations of these Pb isotope ratios using the standard cones assemblage are larger than those using the Jet and X cone assemblage. For example, the internal precision (relative standard error, RSE) of $^{208}Pb/^{204}Pb$ using the standard cones assemblage (1.6%) is two times larger than that using the Jet and X cones assemblage (0.8%) (Fig. 5).

Compared to the standard cones assemblage, the Jet sample cone and X skimmer cone assemblage can improve the external precisions of *in situ* Pb isotope ratios significantly (Fig. 6a and b). Using the Jet and X cones, under the same laser ablation conditions, the precisions for almost all the samples are improved by at least a factor of two compared to using the standard cones. For example, using the standard cones with a 24 μm laser spot the ^{208}Pb signal intensity for TB-1G is ~140 000 cps and the $^{208}Pb/^{206}Pb$ and $^{208}Pb/^{204}Pb$'s precisions are 0.38% and 2.26% (2RSD). When using the Jet and X cones, the ^{208}Pb signal intensity for TB-1G is improved to ~420 000 cps, and the precisions are improved to 0.19% and 1.04% (2RSD) respectively.

Correlation of external precision and signal intensity

In order to obtain a more accurate relationship between data precision and signal intensity, we measured samples with different Pb contents under different laser ablation conditions. The results show that the precisions using the standard cones assemblage and the Jet and X cones assemblage are almost identical at the same signal intensity (since the precisions of $^{207}Pb/^{204}Pb$ and $^{206}Pb/^{204}Pb$ are similar to the precision of $^{208}Pb/^{204}Pb$, only the data of $^{208}Pb/^{204}Pb$ are displayed in Fig. 6). However, using the Jet and X cones can improve the signal intensity by up to two times compared to using the standard cones, which greatly improves precision. For example, using the standard cones, with a 45 μm laser spot, the ^{208}Pb signal intensity of BHVO-2G is only ~48 000 cps and the external precisions for $^{208}Pb/^{206}Pb$ and $^{208}Pb/^{204}Pb$ are 0.44% and 2.07% (2RSD) (Fig. 6c and d). When using the Jet and X cones, under the same laser ablation conditions, the ^{208}Pb signal intensity of BHVO-2G rises to ~134 000 cps and the precisions for $^{208}Pb/^{206}Pb$ and $^{208}Pb/^{204}Pb$ are improved to 0.14% and 1.04%, respectively. The precisions for our measured $^{208}Pb/^{206}Pb$ ratios are much better than the results of Souders and Sylvester[12] while for $^{208}Pb/^{204}Pb$ the precision is similar at the same signal intensity (Fig. 6c and d). This may be caused by the intensity of the ^{204}(Hg + Pb) background, which also was higher with the Jet and X cones assemblage (~4000–9000 cps). From the discussion above we know that under the same laser ablation conditions

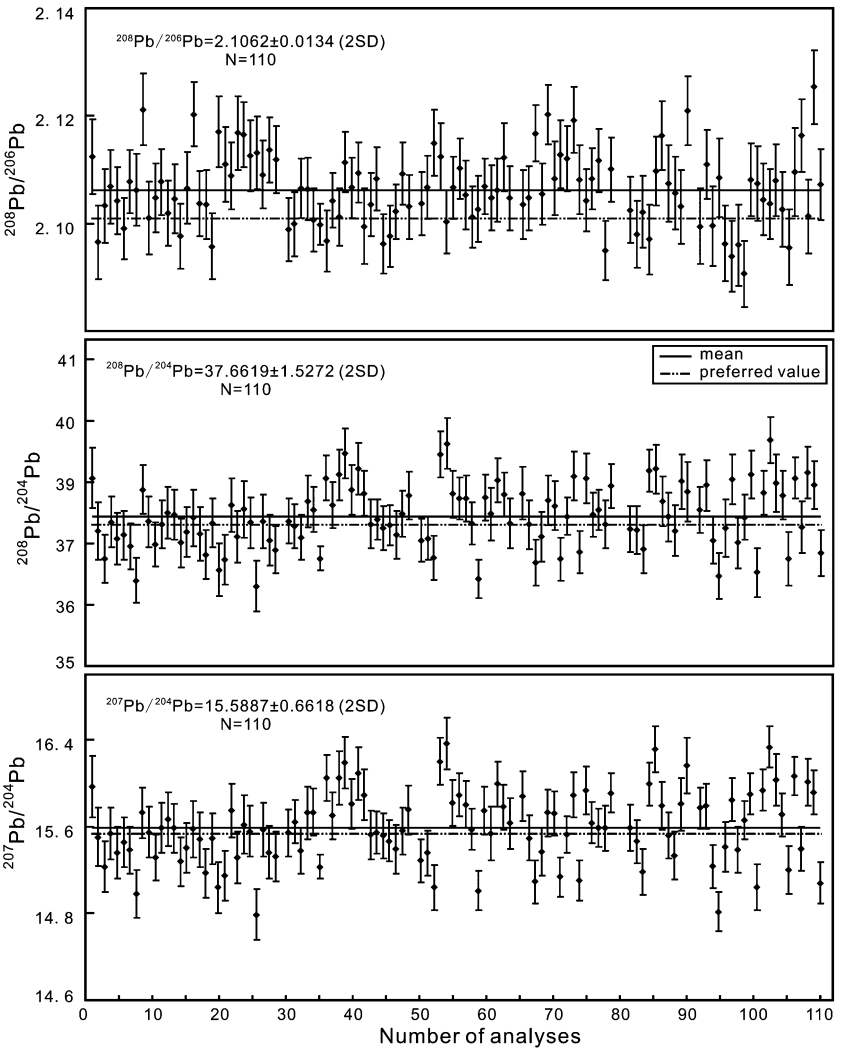

Fig. 4 Pb isotope analysis of NIST 614 using 23 μm laser spot size, 3 Hz repetition rate and 80 mJ energy with a 50% energy attenuator (4 J cm^{-2} energy density). The preferred values are from ref. 21. The error bars correspond to 1 standard error (1SE).

the Jet and X cones assemblage significantly improves the precision compared to the standard cones for the same sample. So replacing the standard cones with Jet and X cones will provide much more precise Pb isotope ratio data compared to the setup of Souders and Sylvester.[12]

Obviously, the precision for experimental data is controlled by many factors, such as sample signal, laser ablation time, instrument conditions and gas blank, and the sample signal is governed by the content of the element of interest, laser ablation parameters (spot size, repetition rate and energy) and instrument sensitivity. For a given sample (such as a melt inclusion), the content of the element of interest is fixed, while for a given laboratory, the instrument sensitivity and gas blank are relatively stable, and thus the instrumental parameters will be the main factor controlling the data precision. Therefore optimization of the instrument parameters for a given sample is crucial. In analyzing inclusions a balance must be obtained between parameter settings that create a high enough signal intensity to have a reasonable precision, but do not result in the laser ablating all the way through the inclusion.

Measurement of natural melt inclusions

We measured Pb isotopes in 429 olivine-hosted melt inclusions from the Cenozoic Hainan Island basalts (219) and the end-Permian Emeishan flood basalts (210). Olivine-hosted melt inclusions are mafic and the compositions and Pb contents are similar to those of NKT-1G and BVHO-2G. Thus both standard glasses have relatively small matrix effects compared to the measured melt inclusions. NKT-1G was selected as the external standard bracketing each melt inclusion measurement. BHVO-2G was analyzed after every five melt inclusion measurements to monitor instrument drift. At the beginning of each analysis session, five pairs of NKT-1G and BHVO-2G were analyzed. After making sure that the corrected Pb isotope ratios of BHVO-2G are within analytical error of the preferred reference values the Pb isotopic compositions of the melt inclusions were measured.

Olivine-hosted melt inclusions from Hainan Island basalts

At first, we adjusted the laser to a 23 μm spot size, 3 Hz repetition rate, and 80 mJ energy with a 50% energy

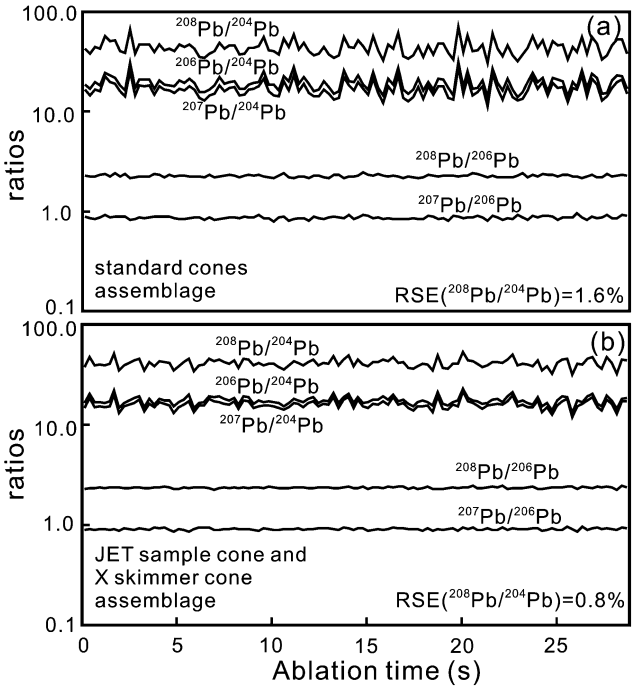

Fig. 5 Variations of Pb isotope ratios during a single spot analysis of NIST 614 using (a) the standard cones assemblage and (b) the Jet sample cone and X skimmer cone assemblage. The same laser parameters (spot size: 23 μm; repetition rate: 3 Hz; energy: 80; energy density: 4 J cm^{-2}) were used in both cases. In the former case, the signal intensity for ^{208}Pb is about 22 000 cps, while in the latter case, it is about 65 000 cps.

attenuator (4 J cm^{-2} energy density) to analyze melt inclusions from the Hainan Island basalts. However, the measurement results showed that the signal intensities of the melt inclusions are very low (the intensity of ^{208}Pb was about 5000–130 000 cps (1300–3400 cps for ^{204}Pb), mostly 20 000–80 000 cps, and the Pb content was estimated to be about 0.1–2.5 μg g^{-1}) under these conditions. At such low intensities the internal precisions of the data for melt inclusions were poor (internal precisions of $^{208}Pb/^{206}Pb$ for most inclusions were larger than 0.40% (2RSE)). To improve the sample signal intensity, we increased the laser spot size to 45 μm. In order to get enough data before the melt inclusions were fully penetrated, a 25% energy attenuator was used. Melt inclusions with diameters larger than 40 μm were analyzed. Under such laser conditions, the sample signal intensity was improved by a factor of two and the internal precision was significantly improved (internal precisions of $^{208}Pb/^{206}Pb$ for most inclusions were less than 0.25% (2RSE)). The average $^{20x}Pb/^{206}Pb$ ratios of BHVO-2G over 3 days are within 0.20% of the preferred values and the ratios involving ^{204}Pb are within 1.0% of the preferred values (Table 6 and Fig. 7). Melt inclusion YX-11-1(3)-8 was large enough (~150 μm) to be ablated three times. These duplicate measurements show excellent agreement. The precisions for $^{208}Pb/^{206}Pb$ and $^{207}Pb/^{206}Pb$ are better than 0.2% (2SD) and for $^{20x}Pb/^{204}Pb$ are better than 1.3% (2SD) (Table 6).

Olivine-hosted melt inclusions from the Emeishan flood basalts

210 olivine-hosted melt inclusions from 9 Emeishan basalts were analyzed with a 45 μm laser spot (this means that about 20–30 melt inclusions in each rock sample were analyzed). Because the Emeishan flood basalts erupted at ~260 Ma the effect of U–Th decay on Pb isotope ratios must be corrected. The following protocol was adopted. The mean gas background intensities were subtracted from the time-resolved signal intensities for each isotope. Then U–Pb and Th–Pb were corrected for elemental fractionation related to pit depth (referred to as downhole fractionation) and the mass bias correction was followed. As shown in many zircon U–Pb dating studies,[30–33] the downhole fractionation of U–Pb is linear with time. In our experiment, the within-analysis laser induced downhole fractionation of $^{238}U/^{206}Pb$ and $^{232}Th/^{206}Pb$ was corrected by applying a linear regression through all measured ratios. Fig. 8 shows typical time-resolved data acquired during laser ablation of the external standard NKT-1G. During the first 22 s, the gas blank was measured with the laser off, followed by 30 s of sample measurement with laser on. The valid data begin at 25 s and end at 55 s. During the laser ablation, as the ablation pit deepens, $^{238}U/^{206}Pb$ and $^{232}Th/^{206}Pb$ decrease linearly with time. Pb is more volatile over U and this leads to preferential volatilization of Pb over U and Th during laser ablation.[32] With the process of laser ablation, the ablation pit gets deeper and the laser energy reaching the sample surface gets less which leads to a stronger Pb and U–Th fractionation. This means that the U–Pb and Th–Pb ratios will get smaller and smaller with the process of laser ablation. We used a linear correlation to calculate both $^{238}U/^{206}Pb$ and $^{232}Th/^{206}Pb$ ratios when the valid data started to be collected (*i.e.*, at 25 s). After the mass bias correction, it is necessary to use U–Pb and Th–Pb decay functions to calculate the Pb isotope ratios of the melt inclusions from the Emeishan flood basalts to the time when they were formed. Due to the low ^{204}Pb intensity of the Emeishan melt inclusions and resultant poor precision, the ratios involving ^{204}Pb were not used. Only the $^{208}Pb/^{206}Pb$ and $^{207}Pb/^{206}Pb$ were calculated to their initial values. The method for calculating initial lead isotope ratios is given in ESI S2.†

The $^{238}U/^{206}Pb$ and $^{232}Th/^{206}Pb$ for the uncorrected Pb isotope ratios are 0.1927–1.3334 and 0.5570–5.0304 respectively. Their $^{208}Pb/^{206}Pb$ and $^{207}Pb/^{206}Pb$ range from 2.0275–2.1014 and 0.8070–0.8426, with mean values 2.0671 and 0.8215, respectively (Fig. 9 and ESI S3†). After U–Th correction, the $^{208}Pb/^{206}Pb$ and $^{207}Pb/^{206}Pb$ of the Emeishan melt inclusions ranging from 2.0610–2.1179 and 0.8330–0.8617, with means of 2.0911 and 0.8445, have deviations of 1.2% and 2.8% with the uncorrected Pb isotope ratios, respectively. This shows the necessity to perform age-corrections for old samples.

Comparison with previous studies

Table 5 presents a summary of results obtained in previous studies, which can be compared with our results in Tables 4 and 6. The detectors used by Paul *et al.*[10] and Kent[11] to measure

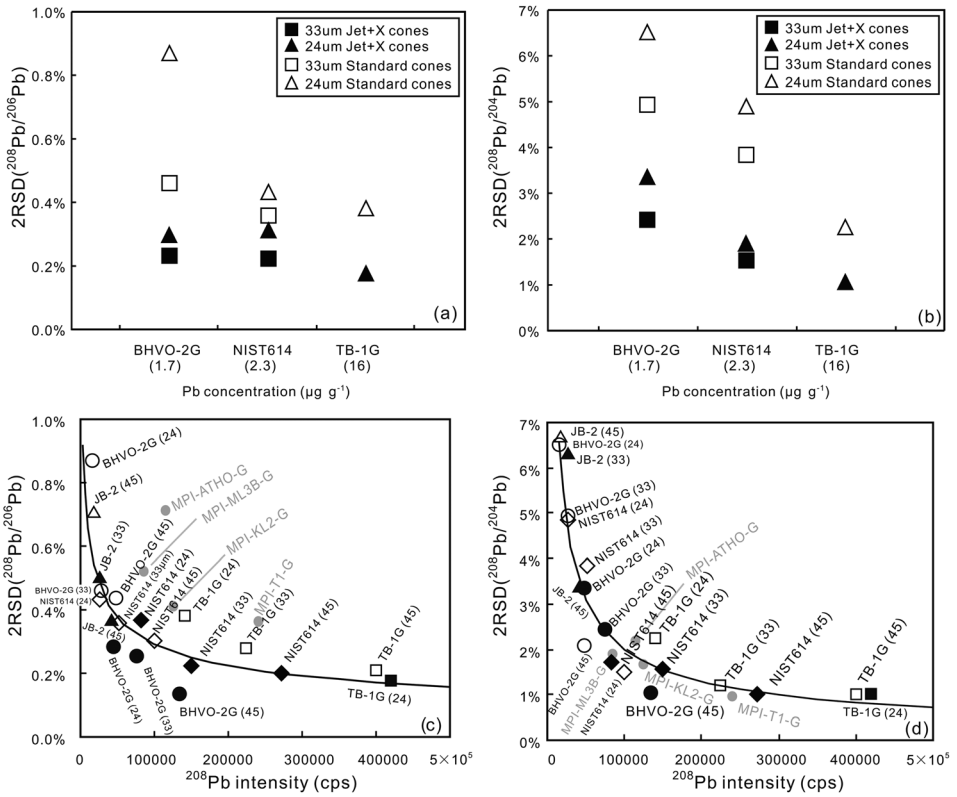

Fig. 6 (a and b) Comparison of the external precision of $^{208}Pb/^{206}Pb$ and $^{208}Pb/^{204}Pb$ using (a) the standard cones assemblage and (b) the Jet and X skimmer cones assemblage. Using the Jet and X cones, under the same laser ablation conditions, the precisions for almost all the samples are improved at least by a factor of two compared to using the standard cones. (c and d) Relationship between external precision and signal intensity for $^{208}Pb/^{206}Pb$ and $^{208}Pb/^{204}Pb$. Filled symbols measured with the Jet and X cones, open symbols measured with the standard cones. The numbers in parentheses show laser spot sizes. The curves are fitted from the experimental data. For the samples in the study of Souders and Sylvester[12] (gray filled circles), we assumed that the signal intensity was proportional to the laser ablation area. Note that at ^{208}Pb signal intensity > 200 000 cps, external precisions of ratios involving ^{204}Pb are better than 1.3% (2RSD) and precisions of $^{208}Pb/^{206}Pb$ and $^{207}Pb/^{206}Pb$ are better than 0.23% (2RSD). All the data in (a–d) were obtained using a 3 Hz repetition rate and 80 mJ energy with a 25% energy attenuator (~2.3 J cm^{-2} energy density). Only the laser spot sizes varied between the different analyses.

Table 6 Lead isotope ratios for melt inclusion YX-11-1(3)-8 in this study[a]

		$^{208}Pb/^{206}Pb$	1SE	$^{207}Pb/^{206}Pb$	1SE	$^{208}Pb/^{204}Pb$	1SE	$^{207}Pb/^{204}Pb$	1SE	$^{206}Pb/^{204}Pb$	1SE
BHVO-2G[b]	Mean (n = 116)	2.0557		0.8336		38.5594		15.6361		18.7568	
	2RSD	0.27%		0.30%		1.45%		1.53%		1.45%	
	Accuracy	0.16%		−0.10%		0.91%		0.65%		0.75%	
YX-11-1(3)-8a		2.0888	0.0015	0.8375	0.0008	38.9711	0.1537	15.6565	0.0640	18.6771	0.0742
YX-11-1(3)-8b		2.0882	0.0013	0.8367	0.0006	39.1371	0.1384	15.6876	0.0547	18.7607	0.0641
YX-11-1(3)-8c		2.0897	0.0016	0.8379	0.0006	38.6568	0.1390	15.5206	0.0547	18.5324	0.0671
	2RSD	0.07%		0.15%		1.25%		1.14%		1.24%	

[a] The laser parameters are 45 μm spot, 3 Hz repetition rate and 80 mJ energy with a 25% energy attenuator (2.3 J cm^{-2} energy density). [b] Preferred reference values for BHVO-2G are from ref. 35.

^{208}Pb, ^{207}Pb and ^{206}Pb are Faraday cups that have much lower sensitivities than ICs. In order to achieve the required signal intensity, both studies used quite large laser spots and 60 s ablation time; these conditions are only suitable for analyzing large melt inclusions. Souders and Sylvester[12] used a smaller laser spot but the laser repetition rate of 10 Hz that they used is too high for most melt inclusion measurements. Using a 24 μm laser spot with a 3 Hz repetition rate, the external precisions for $^{208}Pb/^{206}Pb$ and $^{207}Pb/^{206}Pb$ for almost all standard glasses measured in our study (Fig. 6) are better than the results obtained by SIMS in the study by Saal *et al.*[7] and are comparable to those obtained in the study by Souders and Sylvester.[12] The laser conditions (spot size: 45 μm spot, repetition rate: 3 Hz and 80 mJ energy with a 25% energy

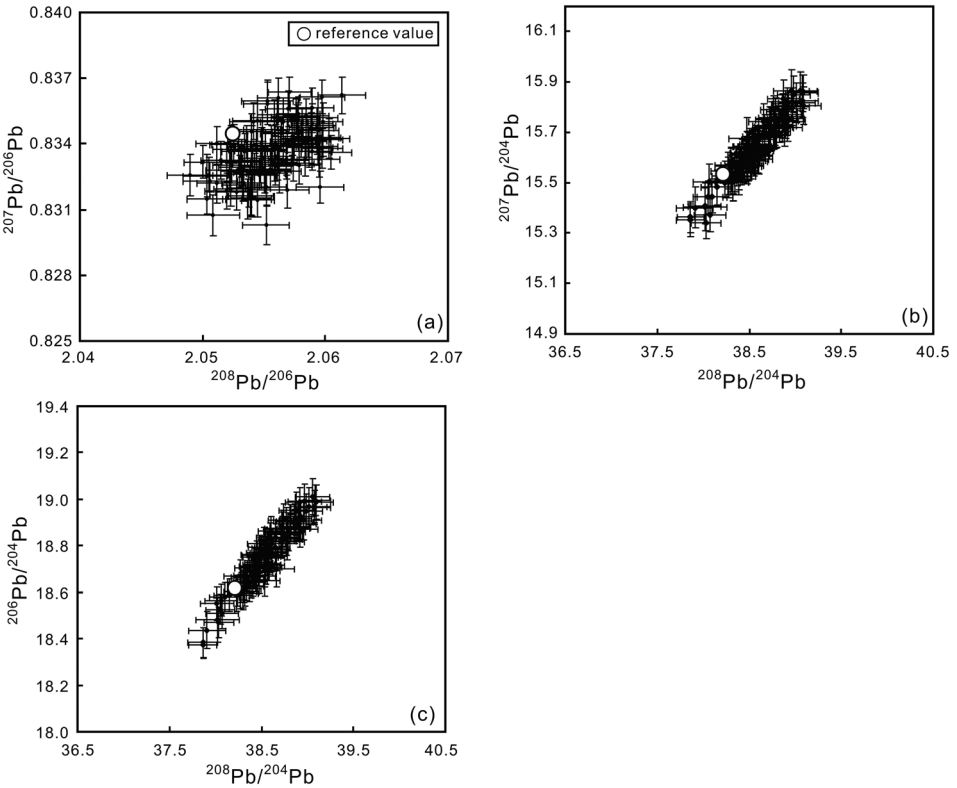

Fig. 7 Pb isotope analysis of BHVO-2G with a 45 μm laser spot size, 3 Hz repetition rate and 80 mJ energy with a 25% energy attenuator (~2.3 J cm^{-2} energy density). The white open circles showing the preferred values fall within the fields defined by the *in situ* analyses. The error bars correspond to 1 standard error (1SE).

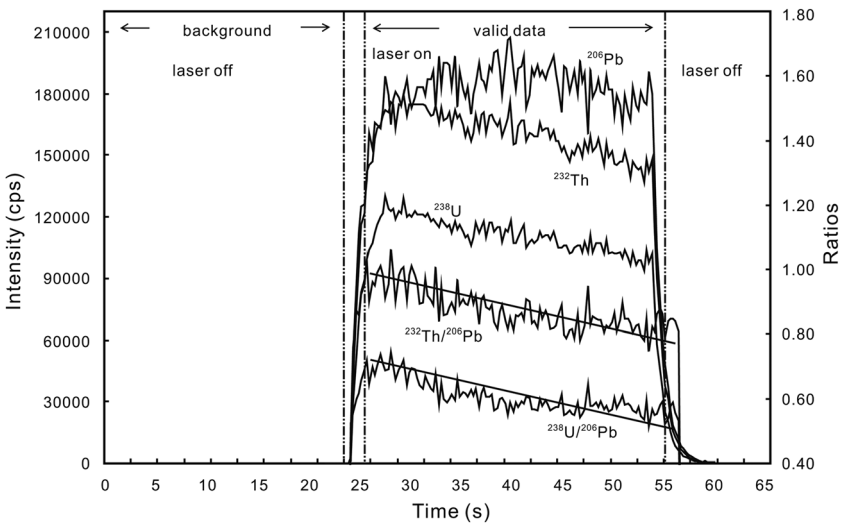

Fig. 8 Representative time-resolved data acquired during laser ablation analysis of NKT-1G. A linear correlation method was used to correct for downhole fractionation.

attenuator (~2.3 J cm^{-2} energy density)) used to analyze natural melt inclusions in this study can be used to measure Pb isotopes in most melt inclusions larger than 40 μm. Compared to the 93 μm laser spot used by Paul *et al.*,[13] our method makes it possible for much smaller melt inclusions to be analyzed for Pb isotopes. What is more, our method collects U and Th data along with the Pb isotopes permitting age-corrections to be performed in melt inclusions from ancient lavas which results in the reduction of the spread of data (Fig. 9). Considering these facts, we suggest that the analytical protocol presented here offers an improvement in Pb isotope analysis compared to previous studies.

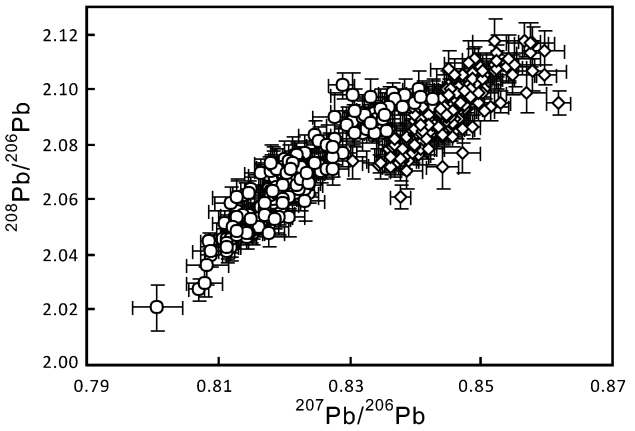

Fig. 9 The Pb isotope ratios for melt inclusions from the Emeishan flood basalt. The small circles are age-uncorrected Pb isotope ratios and the diamonds are age-corrected. The error bars correspond to 2 standard error. The Pb isotope data for the Emeishan melt inclusions are from Ren *et al.* unpublished data.

Conclusions

Under the same laser ablation conditions, using the Jet sample cone and X skimmer cone can improve the sample signal intensity by up to 2 times compared to using standard cones and the precisions of Pb isotopic ratios can be improved at least by a factor of two. The precision of collected data is controlled by many factors. However, for a specific sample and laboratory, the laser conditions, which have a critical effect on the sample signal intensity, act as the main factors controlling the data precision. Therefore optimizing the laser parameters for a specific sample is vital. Optimized laser parameters to analyze Pb isotopes in melt inclusions, using a Jet sample and X skimmer cone, give ^{208}Pb signal intensity >200 000 cps, external precisions of ratios involving ^{204}Pb better than 1.3% (2RSD), and precisions of $^{208}Pb/^{206}Pb$ and $^{207}Pb/^{206}Pb$ better than 0.23% (2RSD). Measurement of melt inclusions from old samples, such as the ~260 Ma Emeishan basalts, shows that it is important to conduct age-corrections in such samples. Compared to previous studies, the laser conditions (spot size: 45 μm spot, repetition rate: 3 Hz and 80 mJ energy with a 25% energy attenuator (~2.3 J cm^{-2} energy density)) used in our protocol are more suitable for most melt inclusion Pb isotope measurements. The method we have developed can provide fast, precise and accurate *in situ* Pb composition analysis, not only for young melt inclusions, but also for old samples that require age-correction for U–Th decay. To improve the precision of $^{20x}Pb/^{204}Pb$ for samples with very low Pb content (<1 μg g^{-1}), further study is needed to improve the sample signal intensity and reduce the Hg gas blank.

Acknowledgements

We would like to thank Wu Lei for kind assistance with sample preparations and LA-MC-ICP-MS measurements. The authors thank three anonymous reviewers for their critical and constructive comments to improve this manuscript. The authors gratefully acknowledge the financial support from the National Basic Research Program of China (2011CB808903), the National Science Foundation of China (91214202, 41172064), and the "hundred talent project" of Chinese Academy of Sciences. This is contribution No. IS-1861 from GIG-CAS.

References

1 A. V. Sobolev, *Petrology*, 1996, **4**, 209–220.
2 L. V. Danyushevsky, F. N. Della-Pasqua and S. Sokolov, *Contrib. Mineral. Petrol.*, 2000, **138**, 68–83.
3 E. Hauri, *Chem. Geol.*, 2002, **183**, 115–141.
4 A. J. R. Kent, *Rev. Mineral. Geochem.*, 2008, **69**, 273–331.
5 V. S. Kamenetsky, A. A. Gurenko and A. C. Kerr, *Geology*, 2010, **38**, 1003–1006.
6 A. E. Saal, S. R. Hart, N. Shimizu, E. H. Hauri and G. D. Layne, *Science*, 1998, **282**, 1481–1484.
7 A. E. Saal, S. R. Hart, N. Shimizu, E. H. Hauri, G. D. Layne and J. M. Eiler, *Earth Planet. Sci. Lett.*, 2005, **240**, 605–620.
8 J. Maclennan, *Geochim. Cosmochim. Acta*, 2008, **72**, 4159–4176.
9 H. Yurimoto, T. Kogiso, K. Abe, H. G. Barsczus, A. Utsunomiya and S. Maruyama, *Phys. Earth Planet. Inter.*, 2004, **146**, 231–242.
10 B. Paul, J. D. Wood and J. Hergt, *J. Anal. At. Spectrom.*, 2005, **20**, 1350–1357.
11 A. J. R. Kent, *J. Anal. At. Spectrom.*, 2008, **23**, 968–975.
12 A. K. Souders and P. J. Sylvester, *J. Anal. At. Spectrom.*, 2008, **23**, 535–543.
13 B. Paul, J. D. Woodhead, J. Hergt, L. Danyushevsky, T. Kunihiro and E. Nakamura, *Chem. Geol.*, 2011, **298**, 210–223.
14 S. M. Eggins, L. P. J. Kinsley and J. M. G. Shelley, *Appl. Surf. Sci.*, 1998, **127–129**, 278–286.
15 S. E. Jackson, N. J. Pearson, W. L. Griffin and E. A. Belousova, *Chem. Geol.*, 2004, **211**, 47–69.
16 M. Tiepolo, C. Bouman, R. Vannuccl and J. Schwieters, *Appl. Geochem.*, 2006, **21**, 788–801.
17 GeoReM, Max-Planck-Institute database for geological and environmental reference materials, http://georem.mpch-mainz. gwdg.de/.
18 GSJ geochemical reference samples database, http://gbank.gsj.jp/geostandards/.
19 S. A. Wilson, Preliminary Certificate of Analysis: Nephelinite, Knippa, Texas, NKT-1G. US Geological Survey Open-File Report, 2006.
20 P. J. Potts, M. Thompson and S. Wilson, *Geostand. Newsl.*, 2002, **26**, 197–235.
21 J. D. Woodhead and J. M. Hergt, *Geostand. Newsl.*, 2001, **25**, 261–266.
22 K. A. Matthews, M. T. Murrell, S. J. Goldstein, A. J. Nunn and D. E. Norman, *Geostand. Geoanal. Res.*, 2011, **35**, 227–234.
23 Z. Y. Ren, S. Ingle, E. Takahashi, N. Hirano and T. Hirata, *Nature*, 2005, **436**, 837–840.
24 A. K. Souders and P. J. Sylvester, Use of multiple channeltron ion counters for LA-MC-ICP-MS analysis of common lead

isotopes in silicate glasses, in *Laser-Ablation-ICPMS in the Earth Science: Principles and Applications*, ed. P. Sylvester, Mineral. Assoc. Can. Short Course Series, 2008, vol. 40, pp. 265–281.
25 K. J. R. Rosman and P. D. P. Taylor, *Pure Appl. Chem.*, 1998, **70**, 217–235.
26 I. V. Chernyshev, A. V. Chugaev and K. N. Shatagin, *Geochem. Int.*, 2007, **45**, 1065–1076.
27 H. K. Cooper, M. J. M. Duke, A. Simonetti and G. C. Chen, *J. Archaeol. Sci.*, 2008, **35**, 1732–1747.
28 K. Newman, P. A. Freedman, J. Williams, N. S. Belshaw and A. N. Halliday, *J. Anal. At. Spectrom.*, 2009, **24**(6), 701–848.
29 Z. C. Hu, Y. S. Liu, S. Gao, W. G. Liu, W. Zhang, X. R. Tong, L. Lin, K. Q. Zong, M. Li, H. H. Chen, L. Zhou and L. Yang, *J. Anal. At. Spectrom.*, 2012, **27**, 1391–1399.
30 P. J. Sylvester and M. Ghaderi, *Chem. Geol.*, 1997, **141**, 49–65.
31 J. Košler, H. Fonneland, P. Sylvester, M. Tubrett and R. B. Pedersen, *Chem. Geol.*, 2002, **182**, 605–618.
32 S. E. Jackson, N. J. Pearson, W. L. Griffin and E. A. Belousova, *Chem. Geol.*, 2004, **211**, 47–67.
33 D. L. Tollstrup, L. W. Xie, J. B. Wimpenny, E. Chin, C. T. Lee and Q. Z. Yin, *Geochem., Geophys., Geosyst.*, 2012, **13**, DOI: 10.1029/2011gc004027.
34 M. Elburg, P. Vroon, B. V. D. Wagt and A. Tchalikian, *Chem. Geol.*, 2005, **223**, 196–207.
35 D. Weis, B. Kieffer, C. Maerschalk, W. Pretorius and J. Barling, *Geochem., Geophys., Geosyst.*, 2005, **6**, DOI: 10.1029/2004gc000852.
36 J. Kimura, T. W. Sisson, N. Nakano, M. L. Coombs and P. W. Lipman, *J. Volcanol. Geotherm. Res.*, 2006, **151**, 51–72.